Photoinduced coherent adsorbate dynamics on a metal surface: Nuclear wave-packet simulation with quasi-diabatic potential energy curves using an open-boundary cluster model approach

Tomokazu Yasuike and Katsuyuki Nobusada[*]

Department of Theoretical and Computational Molecular Science, Institute for Molecular Science, Myodaiji, Okazaki, Aichi 444-8585, Japan and Department of Structural Molecular Science, School of Physical Sciences, The Graduate University for Advanced Studies (SOKENDAI), Myodaiji, Okazaki, Aichi 444-8585, Japan

We present a nuclear wave-packet simulation of photoinduced coherent adsorbate dynamics on a metal surface with quasi-diabatic potential energy curves obtained from our recently developed open-boundary cluster model approach. Photoexcitation to the resonant adsorbate state and the subsequent ultrafast decay to the electronically excited substrate states were found to cause a coherent vibration of the adsorbate on the metal surface. This process competes with a Raman scattering process, which is generally believed to explain the coherent adsorbate vibration. These two mechanisms induce vibrations with a common frequency, and therefore cannot be distinguished from each other in a frequency-domain experiment. However, they can be distinguished by determining the initial vibrational phase through a time domain experiment such as ultrafast pump-probe spectroscopy. We further demonstrate that for near-resonant excitation the oscillation amplitude induced by our proposed mechanism largely exceeds the amplitude due to the Raman mechanism.

PACS number(s): 34.35.+a, 33.35.+r, 73.20.Hb, 68.35.Ja

I. INTRODUCTION

Since the advent of femtosecond lasers in the early 1980s, time-resolved experiments on a wide variety of ultrafast phenomena have been carried out.[1,2] A major focus of this trend has been the excitation and detection of coherent lattice vibrations in various materials, including insulators,[3] semiconductors,[4,5] semimetals,[6,7] and metals.[8] Recently, photoinduced coherent dynamics of adsorbates have also been observed on surfaces.[9–12] This progress has great significance, because it opens the possibility of coherent manipulation of atoms and molecules adsorbed on solid surfaces and has potential applications in heterogeneous photocatalysis and the fabrication of molecular electronic devices. To realize the desired coherent manipulation of adsorbates, it is necessary to understand the mechanisms responsible for causing the coherent dynamics in adsorbate-surface systems. The impulsive stimulated Raman scattering (ISRS) process[13–15] is a general mechanism of coherent wave-packet motion, not only for lattice vibrations but also for intramolecular vibrations in isolated molecules. The off-resonant ISRS process has been accepted as the only conceivable mechanism of coherent adsorbate dynamics on insulating surfaces. However, the mechanism of photoinduced adsorbate dynamics on metal surfaces remains controversial, because the excited electronic states are easily accessible for metal surfaces, and their contributions have not been fully understood. The excited electronic states are intermediate states in the resonant ISRS process, and thus no coherent dynamics occurs in the excited states, whereas the wave-packet dynamics on an excited state itself is observed as coherent dynamics in the displacive excitation of coherent phonons (DECP).[6,7] Alternatively, we have recently pointed out another possibility of the excited state to generate coherent adsorbate dynamics.[16] The excited adsorbate states on metal surfaces have only a very short lifetime. The formation and ultrafast decay of a metastable excited state would trigger coherent dynamics on another electronic state to which the metastable state relaxes.

Adsorbate dynamics on insulating surfaces can be simulated, for example, by following the motion of a nuclear wave-packet on Born-Oppenheimer (BO) potential energy surfaces (PESs) obtained by *ab initio* electronic structure calculations of a model cluster mimicking an adsorbate-surface system.[17] However, such a theoretical approach is difficult to apply to metal systems because there are an infinite number of electronic states near the Fermi level. Even if an adsorbate-surface system could be approximated by a model cluster, it would be necessary to follow the time evolution of a nuclear wave-packet, taking account of nonadiabatic transitions among a number of electronic states.

We have recently developed a generalized cluster model approach applicable to adsorbate-metal surface systems.[18] This approach enables us to properly treat nonequilibrium electronic states, describing the irreversible electron transfer from an adsorbate to a surface. In the approach, we identify the nonequilibrium steady state as the resonance state and impose an outgoing-wave boundary condition (OBC) on the edge of the adsorbate-surface model cluster. Thus, it was named the open-boundary cluster model (OCM) approach. Our method generalizes previous similar approaches[19–21] applicable to a wider class of Hamiltonians. By applying the OCM approach to the Harris-Holloway-Darling model potential[22] of the NO/Pt(111) system, we succeeded in obtaining quasi-diabatically decoupled potential energy curves (PECs) of the electronic states localized on the adsorbate.[18] The nonadiabatic couplings among the obtained PECs have been shown to be negligibly small. The adsorbate dynamics on metal surfaces was simulated by carrying out the time evolution of the nuclear wave-packet on the OCM PECs. From the results of the simulation, we reported that a transient adsorbate plays a key role in the generation of coherent adsorbate dynamics. However, the excitation process was not explicitly treated in our previous letter, and the relative im-

portance between the ISRS and our proposed processes was not discussed. In the present work, we carry out a nuclear wave-packet simulation on the OCM PECs, explicitly including the process of irradiation by a short laser pulse, and discuss differences in the nature of the coherent dynamics generated by both mechanisms. Atomic units are used throughout, unless otherwise stated.

II. COMPUTATIONAL MODEL AND METHOD

A. Quasi-diabatic potential energy curves of an adsorbate-metal surface system

Although the application of the OCM approach to an adsorbate-surface system was described in the previous paper,[16] a brief review is given here so that the present paper is self-contained. In the OCM approach, the imposition of the OBC at the edge of a model cluster is accomplished by applying a complex scaling technique[23] to the model cluster Hamiltonian. The BO-PESs $\epsilon_i(\mathbf{R})$ in the OCM approach are obtained by solving the eigenvalue problems of the complex-scaled time-independent Schrödinger equation (TISE),

$$\hat{H}_{el}(\mathbf{r}e^{i\theta};\mathbf{R})\Psi_i(\mathbf{r}e^{i\theta};\mathbf{R}) = \epsilon_i(\mathbf{R})\Psi_i(\mathbf{r}e^{i\theta};\mathbf{R}), \quad (1)$$

instead of the normal (i.e., nonscaled) TISE,

$$\hat{H}_{el}(\mathbf{r};\mathbf{R})\Psi_i(\mathbf{r};\mathbf{R}) = \epsilon_i(\mathbf{R})\Psi_i(\mathbf{r};\mathbf{R}), \quad (2)$$

where $\mathbf{r}$ and $\mathbf{R}$ denote the electron and nuclear coordinates, respectively. The real parameter θ rotates the electron coordinates in the complex plane and makes the electronic resonance wave functions integrable in the L^2 function space. The BO-PESs of the conventional cluster model (CCM) are obtained by solving Eq. (2). As in the previous study, we employ here the simple adsorbate-surface model proposed by Harris *et al.*[22] The corresponding electronic (complex-scaled) Hamiltonian is given by

$$\hat{H}_{el}(xe^{i\theta},Z) \equiv -\frac{1}{2e^{2i\theta}}\frac{d^2}{dx^2} + V(xe^{i\theta},Z), \quad (3)$$

where x and Z denote, respectively, the one-dimensional (1D) electron coordinate perpendicular to the metal surface and the 1D nuclear coordinate between the center of mass of the adsorbate and the surface. The explicit functional form of $V(x,Z)$ and its computational parameters were given in the previous paper.[16]

The OCM Hamiltonian matrix is constructed with the Colbert-Miller discrete variable representation (DVR),[24] and by diagonalizing it we then obtain the OCM BO-PECs shown in Fig. 1(a). The manifold consisting of the PECs parallel to the lowest one is a discretized set of the continuum electronic states associated with the substrate-to-substrate (SS) excitation. In the energy range above 3.0 eV, one PEC shows different characteristics from this manifold and seems to be diabatically decoupled from it. As described in the previous study,[16] this PEC represents the anionic adsorbate state associated with the substrate–to-adsorbate (SA) excitation. We have confirmed that the nonadiabatic couplings between the anionic adsorbate state and the other adia-
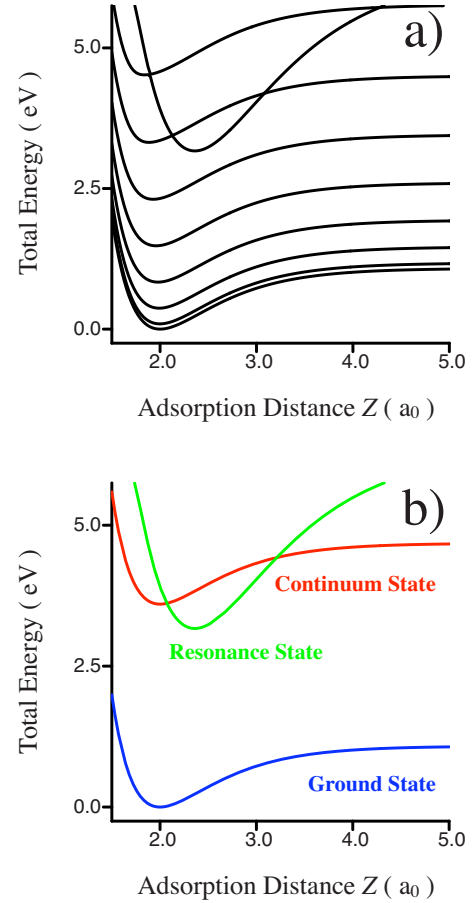

FIG. 1. (Color online) (a) PECs along the adsorption distance Z obtained by the OCM approach. (b) Three-state model derived from the OCM PECs for the ground (blue), resonance (green), and continuum (red) states.

batic PECs in the continuum-state manifold are negligibly small.[16] This anionic state is a resonance state having a complex eigenenergy,[25] namely, a metastable state with a finite lifetime. These features of the anionic adsorbate state are reminiscent of the excited state assumed in the widely accepted phenomenological Menzel-Gomer-Redfield (MGR) model[26,27] of adsorbate-metal surface systems. However, there is an essential difference between the PECs assumed in the MGR model and the ones obtained by the OCM approach. In the MGR model, the background continuum manifold is completely neglected and the model consists of only two electronic states. Therefore, the MGR model implies that the excited state directly relaxes to the ground state. However, it is in general reasonable to consider that relaxation primarily occurs from the excited state to the background continuum manifold, although the continuum states in the manifold eventually relax to the ground state. The imaginary part of the OCM eigenenergy of the anionic adsorbate state is actually related to the rate of relaxation to the background continuum manifold. The importance of the continuum manifold has recently been recognized in several works.[19,21,28–30]

In this sense, a minimal model for adsorbate dynamics on a metal surface should consist of at least three-electronic

states (ground, resonance, and continuum). The number of the continuum states to be included in a single nuclear wave-packet simulation is reduced to one by assuming (i) the nonadiabatic couplings among the continuum states are negligible and (ii) all the PECs of the continuum states are parallel to the ground state PEC. These assumptions are well-satisfied in the obtained OCM PECs and the nuclear dynamics is essentially described by the three-state model shown in Fig. 1(b). The three states included in the model are the ground state (blue curve), the anionic adsorbate resonance state (green curve), and the representative continuum state extracted from the background continuum manifold (red curve). The nuclear dynamics involved with a different continuum state is alternatively simulated using a continuum state PEC shifted by a constant value. A similar three-state model has been used to discuss nuclear dynamics in isolated molecules with decaying electronic states by Cederbaum and co-workers.[31–33]

B. Nuclear dynamics on quasi-diabatic OCM potential energy curves

The nuclear wave-packets of Ψ_g, Ψ_r, and Ψ_c on the ground, the resonance, and the continuum states, respectively, propagate according to the following time-dependent Schrödinger equation,

$$
i\hbar\frac{\partial}{\partial t}\begin{pmatrix}\Psi_r\\\Psi_c\\\Psi_g\end{pmatrix}
$$

$$
=\begin{pmatrix}T+V_r(Z)-i\dfrac{\Gamma(Z)}{2} & 0 & -\mu_{SA}F(t)\\[2mm]\sqrt{\dfrac{\Gamma(Z)}{2\pi}} & T+V_{gs}(Z)+E & -\mu_{SS}F(t)\\[2mm]-\mu_{SA}F(t) & -\mu_{SS}F(t) & T+V_{gs}(Z)\end{pmatrix}
$$

$$
\times\begin{pmatrix}\Psi_r\\\Psi_c\\\Psi_g\end{pmatrix}, \tag{4}
$$

where T is the kinetic-energy operator, $V_r(Z)$ is the PEC of the resonance state, $\Gamma(Z)$ is the Z-dependent decay rate of the resonance state, $F(t)$ is the electric field of the applied laser pulse, and $\mu_{SS}(\mu_{SA})$ is the transition dipole moment for substrate-to-substrate (substrate-to-adsorbate) excitation. The values of μ will be determined in Sec. II C. The applied electric field $F(t)$ is given by

$$
F(t)=F_0\exp\left[-\frac{(t-t_{cen})^2}{2\sigma^2}\right]\cos\Omega(t-t_{cen}), \tag{5}
$$

and

$$
\sigma=\frac{FWHM}{2\sqrt{2\log 2}}, \tag{6}
$$

where FWHM is the full-width at half maximum of the applied pulse, $t_{cen}=2\cdot FWHM$ is its time center, F_0 is the peak value of the field, and Ω is the center frequency. In Eq. (4),

the potential energy curve of the continuum state is given by $V_{gs}(Z)+E$ parallel to $V_{gs}(Z)$. We set E equal to Ω so that the corresponding electronic state could have the largest population among the continuum states.

The time-dependent Schrödinger equation, Eq. (4), is mapped using the position-space grids of Colbert-Miller DVR, and the time evolution of the wave-packet $\Psi \equiv {}^T(\Psi_r,\Psi_f,\Psi_g)$ is carried out using the split operator method as follows:

$$
\Psi(t+\Delta t)=e^{-(i/\hbar)\mathbf{H}\Delta t}\Psi(t)\sim e^{-(i/2\hbar)\mathbf{T}\Delta t}e^{-(i/2\hbar)\mathbf{V}'E(t+\Delta t/2)\Delta t}
$$

$$
\times e^{-(i/\hbar)\mathbf{V}\Delta t}e^{-(i/2\hbar)\mathbf{V}'E(t+\Delta t/2)\Delta t}e^{-(i/2\hbar)\mathbf{T}\Delta t}\Psi(t), \tag{7}
$$

where $\mathbf{T}$, $\mathbf{V}$, and $\mathbf{V}'$ are the representation matrices of the T, V, and V' operators, respectively. These are defined by

$$
\mathcal{T}\equiv\begin{pmatrix}T & 0 & 0\\0 & T & 0\\0 & 0 & T\end{pmatrix}, \tag{8}
$$

$$
\mathcal{V}\equiv\begin{pmatrix}V_r(Z)-i\dfrac{\Gamma(Z)}{2} & 0 & 0\\[2mm]\sqrt{\dfrac{\Gamma(Z)}{2\pi}} & V_{gs}(Z)+E & 0\\[2mm]0 & 0 & V_{gs}(Z)\end{pmatrix}, \tag{9}
$$

and

$$
\mathcal{V}'\equiv\begin{pmatrix}0 & 0 & -\mu_{SA}\\0 & 0 & -\mu_{SS}\\-\mu_{SA} & -\mu_{SS} & 0\end{pmatrix}. \tag{10}
$$

Once the transformation matrices that diagonalize $\mathbf{T}$, $\mathbf{V}$, and $\mathbf{V}'$ are obtained, the time evolution expressed by Eq. (7) can be efficiently performed. The details of the relevant computational procedures have been described in the literature.[34]

C. Transition dipole moments of substrate-to-substrate and substrate-to-adsorbate excitations

To obtain reference values of the transition moments in the dynamical simulation, we carried out *ab initio* electronic structure calculations at the CI-singles level of theory for NO-Pt$_9$, a conventional cluster model mimicking the fcc-hollow-site adsorbed NO/Pt(111) system. The Pt$_9$ cluster consists of two layers, in which the first and second layers have six and three Pt atoms, respectively. The distance between adjacent Pt atoms was set to be 2.774 Å, allowing for the experimental lattice constant of 3.923 Å. The N-O and N-Pt surface distances of 1.225 and 2.045 Å, respectively, were adopted according to the work of Ge and King.[35] The molecular orbitals used for the CI calculation were determined by restricted Hartree-Fock calculations of the cationic cluster, NO-Pt$_9^+$. We used the CDW-type broken-symmetry HF solution, because the symmetric orbitals showed singlet instability. The employed basis sets were MINI (Ref. 36) for the nitrogen and oxygen atoms and the Hay-Wadt's minimal basis set with its effective core potential[37] for the platinum atom. All calculations were performed with a modified ver-
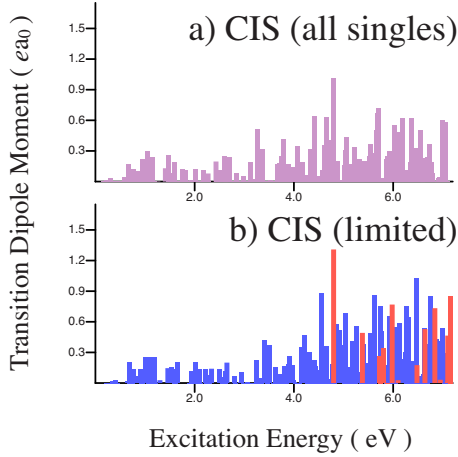
FIG. 2. (Color online) Excitation-energy distribution of the z component of the transition dipole moments for a NO-Pt$_9$ cluster model. The z axis is normal to the surface. (a) All single excitations are included. (b) Limited single excitations are included. The blue and the red bars indicate the SA and the SS excitations, respectively.

sion of the GAMESS quantum chemistry program package.[38]

The excitation-energy distribution of the computed transition dipole moments is shown in Fig. 2 for the lowest 250 excitations from the ground state. Although the results shown in Fig. 2(a) include the effects of the all-single excitations, the nature of each excitation is difficult to assign because its excited state is a complicated mixture of the Slater determinants. To characterize the nature of each excitation, the limited CI-singles calculation was also carried out and the results are shown in Fig. 2(b). As clearly seen from the figure, the general features of Fig. 2(a) remain unchanged, even in the spectrum obtained from the limited CI-singles calculation. The blue and red lines indicate the SA and SS excitations, respectively. No contribution from the adsorbate-to-adsorbate excitation is found in the energy region considered. We can conclude from Fig. 2(b) that the transition dipole moments of the SA excitation are generally larger than those of the SS excitation. We assume $\mu_{SA}=1.0$ and $\mu_{SS}=0.0$ for the following dynamical simulation. This approximation allows us to decouple different continuum states from each other[21] and validates the three-state model given by Eq. (4) as a simple adsorbate dynamics model. Our computational model is significantly simplified. We emphasize that the scope of the present paper is to gain a general understanding of the photoinduced adsorbate dynamics on metal surfaces, rather than perform a quantitative analysis of the dynamics in the NO@Pt(111) system.

III. LASER-INDUCED ADSORBATE DYNAMICS

A. Coherent vibrational excitation by formation and ultrafast decay of metastable adsorbate

To give a simple picture of the adsorbate dynamics, we first consider the resonant excitation. Let us calculate the absorption spectrum using the formula,
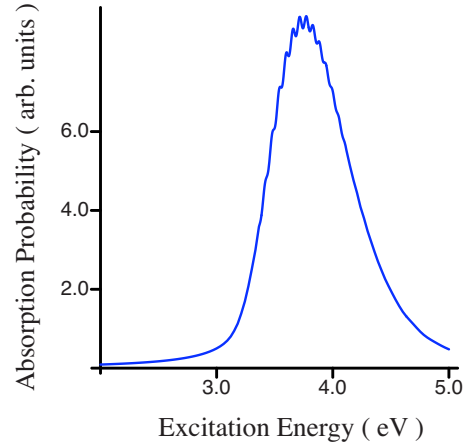

FIG. 3. (Color online) Absorption spectrum for the SA excitation.

$$\sigma(\Omega) \sim -\frac{1}{\pi}\mathrm{Im} \sum_{v_r} \frac{(0_g|v_r)(v_r|0_g)}{\Omega - (E_{v_r} - E_{0_g})}, \qquad (11)$$

$|0_g)$ and E_{0_g} are respectively the wave function and the eigenenergy of the vibrational ground state on the ground electronic state, whereas $|v_r)$ and E_{v_r} are those of the vibrational v-th state on the resonance electronic state. The round bracket indicates that the c product[23] should be performed as the inner product, because $|v_r)$ is a vibrational resonance state. Figure 3 shows the absorption spectrum for the SA excitation and the maximum peak is at 3.77 eV. We carried out the nuclear wave-packet simulation by setting the center energy of the applied laser pulse to the peak energy. The peak electric field F_0 and the pulse FWHM are set to 1.688×10^{-3} au and 15 fs, respectively.

Figure 4 shows the time evolution of the wave-packets moving on the PECs of the ground, resonance, and continuum states after applying the laser pulse. In the early-time region, the ground-state population partially transfers to the resonance state because of the resonant excitation. Then, the wave-packet Ψ_r moves toward the longer adsorption-
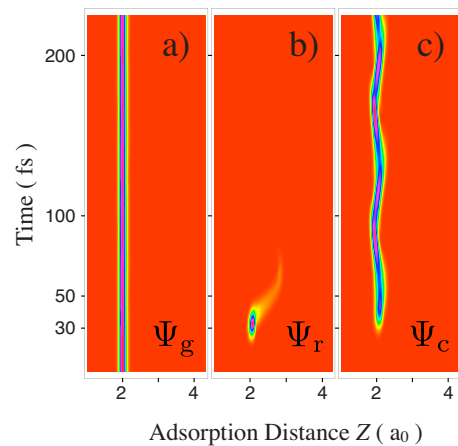

FIG. 4. (Color online) Photoinduced wave-packet dynamics of $\Psi_g(t)$ on the ground state, $\Psi_r(t)$ on the resonance state, and $\Psi_c(t)$ on the continuum state with $E=\Omega$.
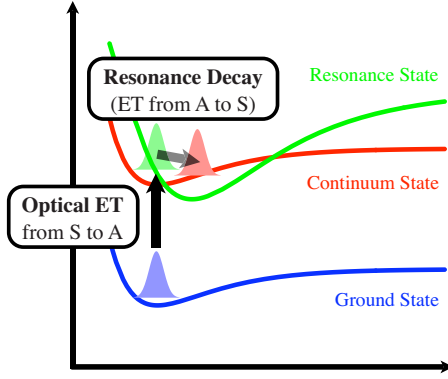
FIG. 5. (Color online) Schematic diagram of the TAM mechanism of causing coherent vibrational motion of the adsorbate on the continuum state.

FIG. 6. (Color online) Time evolution of the expectation values of the adsorption distance, $\langle Z(t) \rangle_i$ (i=g and c). The points indicate the values directly calculated by the time-dependent wave-packets. The continuous curves are the functions, $z_g(t)$ and $z_c(t)$, obtained by fitting those values. The values $\langle Z(t) \rangle_i$ for $t < 60$ fs were ignored in the fitting procedure.

distance region, driven by the slope of the PEC associated with the real part of the resonance energy, with a decrease in the population due to the imaginary part of the resonance energy. This population decay of the resonance state was physically caused by irreversible electron transfer from the adsorbate to the substrate and involves a population transfer to the continuum state. It should be noted that oscillatory motion was not observed on the resonance-state PEC because of the short lifetime of the resonance state. Thus, the DECP mechanism is improbable in the present system. The wave-packet Ψ_c on the continuum-state PEC, generated by fast, irreversible electron transfer, shows an oscillatory behavior, as shown in Fig. 4(c). These processes are schematically drawn in Fig. 5.

The oscillation originates from the nature of coherence in the transferred wave-packet. The initial wave-packet is the vibrational ground state of the electronic ground state and is excited to the resonance state, keeping its Gaussian shape during the short-pulse laser excitation. Then, the position and momentum of the wave-packet on the resonance-state PEC are altered, but its shape does not change significantly during the propagation since the lifetime of the resonance state is only a few femtoseconds, much shorter than the time scale of the nuclear vibrational motion. When this wave-packet transfers to the continuum state, it behaves as a coherent state. This is because the coherent state can be generally produced by altering the position and momentum of the vibrational ground state, and the PECs of the ground and continuum states are similar in shape. For these reasons, the coherent vibrational motion of the nuclear wave-packet on the continuum-state PEC is caused by the formation and subsequent ultrafast decay of the transient adsorbate. We refer to this process as the transient-adsorbate mediation (TAM) mechanism. Although the role of the transient adsorbate has been discussed in regard to the DIET (Refs. 26, 27, 40, and 41) or DIMET (Refs. 39–41) (desorption induced by electronic transition or multiple electronic transitions) mechanism of photoinduced desorptions on metal surfaces, the importance of the TAM mechanism has not been suggested in the context of generating coherent vibrational motion of the adsorbate.

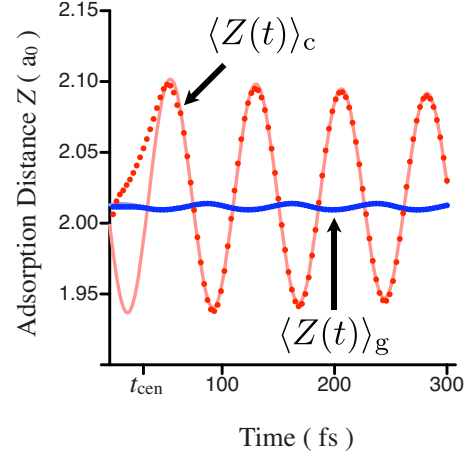It should be mentioned that the wave-packet on the ground-state PEC also showed a very small amplitude oscillation. This oscillation was caused by the ISRS process,[13–15] which has been recognized as a mechanism of generating photoinduced coherent vibrations in adsorbate-surface systems.

To quantitatively compare these competing oscillations on the different PECs, we calculate the expectation values of Z for the ground and continuum states. These expectation values are defined as

$$\langle Z(t) \rangle_g = \frac{\langle \Psi_g(t)|Z|\Psi_g(t) \rangle}{\langle \Psi_g(t)|\Psi_g(t) \rangle} \equiv \frac{\langle \Psi_g(t)|Z|\Psi_g(t) \rangle}{\rho_g(t)} \qquad (12)$$

and

$$\langle Z(E,t) \rangle_c = \frac{\langle \Psi_c(E,t)|Z|\Psi_c(E,t) \rangle}{\langle \Psi_c(E,t)|\Psi_c(E,t) \rangle} \equiv \frac{\langle \Psi_c(E,t)|Z|\Psi_c(E,t) \rangle}{\rho_c(E,t)}, \qquad (13)$$

where $\rho_g(t)$ and $\rho_c(E,t)$ are the time-dependent populations in the ground and the continuum states, respectively. Then, the time profiles of the expectation value of Z are fitted by a function $z(t)$,

$$z(t) = a \exp[-t/\tau_{deph}]\cos[\omega(t - t_{cen}) + \phi] + \tilde{z}, \qquad (14)$$

where a is the initial vibrational amplitude, τ_{deph} is the dephasing time, ω is the vibrational frequency, and ϕ is the initial vibrational phase. Figure 6 shows the expectation values, $\langle Z(t) \rangle_g$ and $\langle Z(\Omega,t) \rangle_c$, and the functions, $z_g(t)$ and $z_c(t)$, fitting those values. As is clearly shown, the initial phases are different from each other, whereas their frequencies are nearly the same. Therefore, the time domain experiments are suitable for the study of the generation mechanism of the coherent vibrational motion. Chesnoy and Mokhtari[14] showed, using a model system consisting of two harmonic PECs that the initial phase of the ground state oscillation by the ISRS mechanism was π for the resonant excitation. The present value of $\phi_g = 0.55\pi$ for the ground state largely de-

viates from π. This deviation partially results from a difference in the definition of the resonant excitation. We defined it by the vertical excitation energy, whereas Chesnoy and Mokhtari used the adiabatic excitation energy. The adiabatic excitaiton energy is generally lower than the vertical excitation energy and is 3.17 eV in the present model. Nevertheless, the obtained value of $\phi_g = 1.32\pi$ for $\Omega = 3.17$ eV still deviates significantly from π. We found that the excitation energy giving $\phi_g = \pi$ lies between the adiabatic and vertical resonant excitation energies in the present simulation. In discussion by Chesnoy and Mokhtari, the excitation field was assumed to be the δ function of t, and thus, their resonance condition does not seem to be well-defined.

The obtained value of $\phi_c = 1.41\pi$ for the continuum state is largely different from ϕ_g, and hence the TAM mechanism can be clearly distinguished from the ISRS mechanism by time domain experiments. $\langle Z(t) \rangle_c$ has an oscillatory behavior such as $\sin(\omega t)$ for $\phi_c = 1.41\pi$. The reasons for this behavior are that the lifetime of the anionic resonance state is very short and the oscillation on the continuum state starts from nearly the original equilibrium adsorption distance.

B. Initial vibrational amplitudes of oscillations induced by ISRS and TAM mechanisms

In the last section, we have compared the time evolutions of the expectation values of Z for the wave-packets on the ground and continuum states. However, to reveal which oscillation is more easily observed experimentally, we must analyze their contributions from the ground and continuum states to the total expectation value of Z,

$$\langle Z(t) \rangle \equiv \langle \Psi_g(t)|Z|\Psi_g(t) \rangle + \langle \Psi_r(t)|Z|\Psi_r(t) \rangle$$
$$+ \int_0^\infty dE \langle \Psi_c(E,t)|Z|\Psi_c(E,t) \rangle \quad (15)$$

$$= \rho_g(t)\langle Z(t) \rangle_g + \rho_r(t)\langle Z(t) \rangle_r + \int_0^\infty dE \rho_c(E,t)$$
$$\times \langle Z(E,t) \rangle_c. \quad (16)$$

Because of its short lifetime, the population of the adsorbate resonance state $\rho_r(t)$ rapidly becomes zero. Then, $\rho_g(t)$ takes a constant value ρ_g and the population conservation law is given by

$$\rho_g + \int_0^\infty dE \rho_c(E,t) = 1. \quad (17)$$

Moreover, the energy dependence of the continuum state population $\rho_c(E,t)$ is known to be approximately proportional to a Lorentzian function,

$$\rho_c(E,t) \sim \frac{1}{\pi} \frac{\gamma/2}{(E-\epsilon)^2 + (\gamma/2)^2}, \quad (18)$$

on a short time scale.[32] In the present simulation, we observed a Lorentzian form of $\rho_c(E,t)$ in the time scale determining the initial phase of the oscillation. The parameters ϵ and γ of the Lorentzian function are approximately the exci-

tation energy Ω and the energy width Γ of the adsorbate resonance state, respectively. Equations (17) and (18) lead to the relationship of

$$\rho_c(E,t) = \frac{1-\rho_g}{\pi} \frac{\gamma/2}{(E-\epsilon)^2 + (\gamma/2)^2}. \quad (19)$$

Here, $\langle Z(E,t) \rangle_c$ weakly depends on E in the energy interval between $\Omega - \Gamma/2$ and $\Omega + \Gamma/2$ and is thus assumed to be constant with respect to E. We then, employ the constant $\langle Z(\Omega,t) \rangle_c$ and finally rewrite $\langle Z(t) \rangle$ by

$$\langle Z(t) \rangle = \rho_g \langle Z(t) \rangle_g + (1-\rho_g)\langle Z(\Omega,t) \rangle_c. \quad (20)$$

Using this expression, we can avoid time-consuming dynamical simulations for different continuum states in calculating $\langle Z(t) \rangle$ and easily understand that the amplitudes of the ISRS- and TAM-induced oscillations, A_{ISRS} and A_{TAM}, are given by

$$A_{ISRS} = \rho_g a_g \quad (21)$$

and

$$A_{TAM} = (1-\rho_g)a_c, \quad (22)$$

where a_g and a_c are the initial amplitudes derived for $\langle Z(t) \rangle_g$ and $\langle Z(\Omega,t) \rangle_c$, respectively.

For the resonant excitation discussed in Sec. III A, we obtained $\rho_g = 0.949$, $a_g = 0.0021$, and $a_c = 0.084$ from the dynamical simulation and derived $A_{ISRS} = 0.0021$ and $A_{TAM} = 0.0043$. The oscillation amplitude induced by the TAM mechanism is larger than that by the ISRS one. Therefore, the TAM mechanism should contribute significantly to the coherent adsorbate oscillation under resonant excitation.

C. Excitation-energy dependence of initial vibrational phase and initial vibrational amplitude

In Secs. III A and III B, we compared the initial vibrational phases and amplitudes of the oscillations induced by the ISRS and TAM mechanisms under resonant excitation. However, the excitation energy is usually limited by the available lasers, and thus we next examine the excitation-energy dependence of these properties. Figure 7(a) shows the excitation-energy dependence of the initial vibrational phases, ϕ_g (blue solid curve) and ϕ_c (red solid curve), of the oscillations induced in the ground and the continuum states, respectively. When the center energy of the applied laser pulse Ω increases from 2.7 eV, ϕ_g gradually decreases from $\sim 3\pi/2$ across the value of π near the resonance energy. In other words, the oscillation on the ground state generated by the ISRS mechanism shows a sinelike behavior for the off-resonant excitation, whereas it displays a cosinelike behavior for the near-resonant excitation. These features are in qualitative agreement with the ISRS theory of Chesnoy and Mokhtari.[14] In contrast, the oscillation on the continuum state induced by the TAM mechanism gives different behavior. Although the initial vibrational phase ϕ_c also decreases with increasing Ω, it starts from $\sim 2\pi$ at $\Omega = 2.7$ eV and crosses the value of $3\pi/2$ near the resonance energy. This means that cosine and sinelike oscillations are induced by the
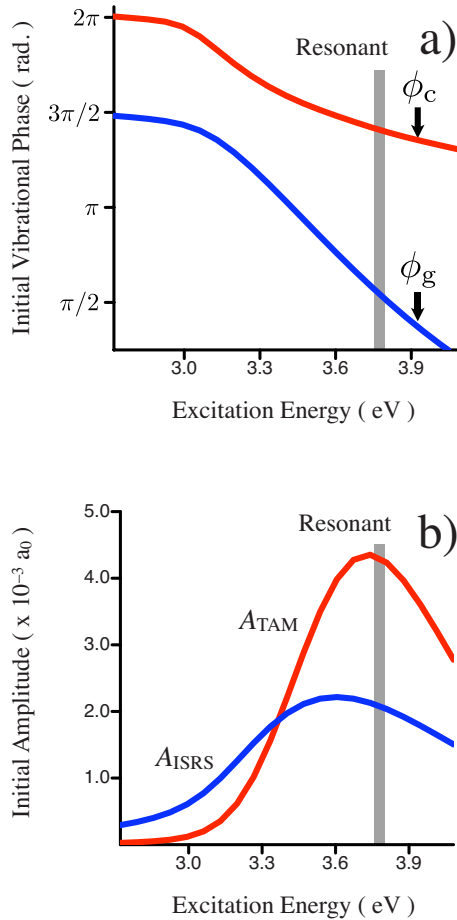
FIG. 7. (Color online) (a) Excitation-energy dependence of the initial vibrational phase, ϕ_i (i=g and c). (b) Excitation-energy dependence of the initial amplitude, A_i (i=ISRS and TAM).

off- and on-resonant excitations, respectively. This relationship in the oscillation induced by the TAM mechanism is opposite to that in the oscillation induced by the ISRS mechanism. Therefore, the oscillations induced by these mechanisms are distinguishable from each other by the difference in their initial vibrational phases, which are measurable in time domain experiments, irrespective of the excitation energy.

As indicated by Eq. (22), the initial amplitude of the oscillation induced by the TAM mechanism depends on the population integrated over the continuum states $1-\rho_g$ and is expected to have a small value for off-resonant excitation. To quantitatively specify the excitation-energy region where the TAM process predominates over the ISRS process, we study

the excitation-energy dependence of the initial vibrational amplitudes for both mechanisms. The results are shown in Fig. 7(b). The blue and the red solid curves represent the initial vibrational amplitudes, A_{ISRS} and A_{TAM}, of the oscillations induced by the ISRS and TAM mechanisms, respectively. Although both amplitudes of A_{ISRS} and A_{TAM} are enhanced near the resonant energy, the enhancement is more remarkable for the oscillation induced by the TAM mechanism and A_{TAM} is larger than A_{ISRS} over a wide energy range near the resonant excitation energy.

On the basis of the excitation-energy dependence of the initial vibrational phases and amplitudes, we propose that the experimentally observed oscillation behavior should be fitted by two functions with the form of Eq. (14). Such an analysis enables us to quantitatively distinguish the competing ISRS and TAM processes and gives a deeper insight into the understanding of adsorbate dynamics on metal surfaces.

IV. CONCLUSION

We have applied the OCM approach, recently developed by the authors, to the model of an adsorbate-metal surface system proposed by Harris *et al.* to obtain quasi-diabatic PECs. Using a three-state model based on the quasi-diabatic PECs, a nuclear wave-packet simulation of photoexcited adsorbate-metal surface dynamics has been carried out at a low computational cost. We have found that the transient adsorbate plays a key role in causing coherent vibrational motion of the adsorbate and have demonstrated that the TAM mechanism would be important in actual experiments. When the direct electronic transition from the ground electronic state to the background continuum manifold is negligible, the TAM process can be decisively distinguished from the conventional ISRS process by determining the initial vibrational phase, which is routinely measured in recent time domain experiments. Therefore, the importance of our proposed TAM mechanism will be demonstrated. We believe that dynamics simulations in real systems using the *ab initio* OCM PESs and corresponding time domain experiments complement each other to give us a quantitative understanding of photoinduced adsorbate dynamics on metal surfaces.

*Author to whom correspondence should be addressed; nobusada@ims.ac.jp

[1] L. Dhar, J. A. Rogers, and K. A. Nelson, Chem. Rev. **94**, 157 (1994).

[2] J. C. Polanyi and A. H. Zewail, Acc. Chem. Res. **28**, 119 (1995).

[3] K. Ishioka, M. Hase, M. Kitajima, and H. Petek, Appl. Phys. Lett. **89**, 231916 (2006).

[4] G. C. Cho, W. Kütt, and H. Kurz, Phys. Rev. Lett. **65**, 764 (1990).

[5] A. Rousse, C. Rischel, S. Fourmaux, I. Uschmann, S. Sebban, G.

Grillon, Ph. Balcou, E. Foerster, J. P. Geindre, P. Audebert, J. C. Gauthier, and D. Hulin, Nature (London) **410**, 65 (2001).

[6] T. K. Cheng, J. Vidal, H. J. Zeiger, G. Dresselhaus, M. S. Dresselhaus, and E. P. Ippen, Appl. Phys. Lett. **59**, 1923 (1991).

[7] H. J. Zeiger, J. Vidal, T. K. Cheng, E. P. Ippen, G. Dresselhaus, and M. S. Dresselhaus, Phys. Rev. B **45**, 768 (1992).

[8] M. Hase, K. Ishioka, J. Demsar, K. Ushida, and M. Kitajima, Phys. Rev. B **71**, 184301 (2005).

[9] H. Petek, M. J. Weida, H. Nagano, and S. Ogawa, Science **288**, 1402 (2000).

[10] K. Watanabe, N. Takagi, and Y. Matsumoto, Chem. Phys. Lett. **366**, 606 (2002).

[11] K. Watanabe, N. Takagi, and Y. Matsumoto, Phys. Rev. Lett. **92**, 057401 (2004).

[12] Y. Matsumoto and K. Watanabe, Chem. Rev. **106**, 4234 (2006).

[13] Y.-X. Yan, E. B. Gamble, and K. A. Nelson, J. Chem. Phys. **83**, 5391 (1985).

[14] J. Chesnoy and A. Mokhtari, Phys. Rev. A **38**, 3566 (1988).

[15] V. Romero-Rochin and J. A. Cina, Phys. Rev. A **50**, 763 (1994).

[16] T. Yasuike and K. Nobusada, Chem. Phys. Lett. **457**, 241 (2008).

[17] T. Klüner, H.-J. Freund, J. Freitag, and V. Staemmler, J. Chem. Phys. **104**, 10030 (1996).

[18] T. Yasuike and K. Nobusada, Phys. Rev. B **76**, 235401 (2007).

[19] Z. W. Gortel, R. Teshima, and H. J. Kreuzer, Phys. Rev. B **37**, 3183 (1988).

[20] T. Klamroth and P. Saalfrank, Surf. Sci. **410**, 21 (1998).

[21] N. Shenvi, H. Cheng, and J. C. Tully, Phys. Rev. A **74**, 062902 (2006).

[22] S. M. Harris, S. Holloway, and G. R. Darling, J. Chem. Phys. **102**, 8235 (1995).

[23] N. Moiseyev, Phys. Rep. **302**, 212 (1998).

[24] D. T. Colbert and W. H. Miller, J. Chem. Phys. **96**, 1982 (1992).

[25] A. J. F. Siegert, Phys. Rev. **56**, 750 (1939).

[26] D. Menzel and R. Gomer, J. Chem. Phys. **41**, 3311 (1964).

[27] P. A. Redhead, Can. J. Phys. **42**, 886 (1964).

[28] T. Seideman, J. Chem. Phys. **106**, 417 (1997).

[29] T. Klamroth, D. Kröner, and P. Saalfrank, Phys. Rev. B **72**, 205407 (2005).

[30] J. P. Gauyacq and A. K. Kazansky, Surf. Sci. **601**, 5473 (2007).

[31] L. S. Cederbaum and F. Tarantelli, J. Chem. Phys. **98**, 9691 (1993).

[32] E. Pahl, H.-D. Meyer, and L. S. Cederbaum, Z. Phys. D: At., Mol. Clusters **38**, 215 (1996).

[33] E. Pahl, H.-D. Meyer, L. S. Cederbaum, and F. Tarantelli, J. Electron Spectrosc. Relat. Phenom. **93**, 17 (1998).

[34] T.-S. Chu and K.-L. Han, J. Phys. Chem. A **109**, 2050 (2005).

[35] Q. Ge and D. A. King, Chem. Phys. Lett. **285**, 15 (1998).

[36] J. Andzelm, M. Klobukowski, E. Radzio-Andzelm, Y. Sakai, and H. Tatewaki, in *Gaussian Basis Sets for Molecular Calculations*, edited by S. Huzinaga (Elsevier, Amsterdam, 1984).

[37] P. J. Hay and W. R. Wadt, J. Chem. Phys. **82**, 299 (1985).

[38] M. W. Schmidt, K. K. Baldridge, J. A. Boatz, S. T. Elbert, M. S. Gordon, J. H. Jensen, S. Koseki, N. Matsunaga, K. A. Nguyen, S. Su, T. L. Windus, M. Dupuis, and J. A. Montgomery, J. Comput. Chem. **14**, 1347 (1993).

[39] J. A. Misewich, T. F. Heinz, and D. M. Newns, Phys. Rev. Lett. **68**, 3737 (1992).

[40] J. C. Tully, Annu. Rev. Phys. Chem. **51**, 153 (2000).

[41] P. Saalfrank, Chem. Rev. **106**, 4116 (2006).